

First measurement of the Hubble constant from gravitational wave-galaxy cross-correlations

Isabela Santiago de Matos^{1,2,*}, Charles Dalang^{3,1,4,†}, Tessa Baker^{1,‡},
Raul Abramo^{5,§}, João Ferri^{5,¶} and Miguel Quartin^{6,7,8,**}

¹*Institute of Cosmology and Gravitation, University of Portsmouth, United Kingdom*

²*ICTP South American Institute for Fundamental Research, São Paulo, Brazil*

³*Institut Philippe Meyer, Département de Physique,*

École Normale Supérieure (ENS), Université PSL, Paris, France

⁴*Queen Mary University of London, United Kingdom*

⁵*Instituto de Física, Universidade de São Paulo, Brazil*

⁶*Centro Brasileiro de Pesquisas Físicas, 22290-180, Rio de Janeiro, RJ, Brazil*

⁷*Observatório do Valongo, Universidade Federal do Rio de Janeiro, 20080-090, Rio de Janeiro, RJ, Brazil*

⁸*PPGCosmo, Universidade Federal do Espírito Santo, 29075-910, Vitória, ES, Brazil*

(Dated: December 18, 2025)

We measure for the first time the Hubble constant (H_0) from the cross-correlation of galaxies and gravitational waves (GW), by applying the *Peak Sirens* method. This method consists of finding the peak of the 3D angular cross-spectrum $C_\ell(z, D_L)$ between the galaxy redshifts (z) and the GW luminosity distances (D_L). Using two GW events from the GWTC-3.0 catalog and the GLADE+ galaxy catalog, we make the first detection of the cross-correlation peak at 5.9σ confidence. This signal comes mostly from the best localized event in the catalog, GW190814, which alone provides a 3.4σ significance. Adding also the multimessenger event GW170817, but without using its known redshift, we find $H_0 = 67^{+18}_{-15}$ km s⁻¹Mpc⁻¹ and the first observational constraint on the GW bias, $b_{\text{gw}} < 4.3$ at 95% CI. These measurements set the stage for future novel cosmological constraints with this technique.

Introduction. The past decade of gravitational wave (GW) observations has opened previously uncharted regimes of gravity, cosmology, and astrophysics [1, 2]. For the new field of GW cosmology, the primary focus to date has been constraints on the luminosity distance-redshift relation, which is sensitive to both cosmological parameters and departures from General Relativity (GR) on cosmological scales. Such constraints are possible because gravitational waveforms from compact binary coalescences (CBCs) inherently yield the luminosity distance D_L of the source (but not its redshift z); this is in contrast with most electromagnetic (EM) sources, whose redshifts, unlike their distances, are generally straightforward to measure.

Several techniques have been proposed to recover the redshifts of GW sources, with most effort focused on bright siren [3–9] and dark siren methods [3, 10–13]. At present, the multimessenger event GW170817 remains the only confirmed bright siren [14, 15]. Consequently, the dark siren method has risen to become the current workhorse of GW cosmology – see applications to real data in [16–29]. In particular, the most recent bound on the Hubble constant (H_0) obtained by LIGO-Virgo-KAGRA (LVK) [30–35] from a combined dark+bright siren analysis of GWTC-4.0 [36–38] together with the GLADE+ galaxy catalog [39] is: $H_0 = 76.6^{+13.0}_{-9.5}$ km s⁻¹Mpc⁻¹ at 68.3% confidence interval (CI) [29].

In this work we apply to current data a third, different technique for associating redshift information to GW sources: GW-galaxy cross-correlation. Several variants of this technique exist [40–49], but in particular

we adopt the *Peak Sirens* method put forward in [50], which draws upon on the original work of [51], an idea akin to the photometric redshift calibration of [52]. The Peak Sirens method uses the fact that the spatial correlations between GW events and galaxies, measured in terms of the angular cross-spectrum, peak when the redshifts of galaxies correspond to the luminosity distances of the GW hosts. Like other standard siren methods, Peak Sirens bypasses the need for external distance calibrations, making it a promising avenue for tackling the Hubble tension [53]; the position of the peak was also shown in [50] to be a robust, model-independent cosmic standard ruler which is insensitive to the precise shape of the matter power spectrum.

The Peak Sirens method allows constraints on the bias of GW sources (b_{gw}), a number quantifying the extent to which GW sources trace the underlying dark matter field. This is a point of difference with current dark sirens approaches, which do not have direct sensitivity to b_{gw} .

Another crucial point of difference with the dark sirens method is that the Peak Sirens technique does not rely on assumptions about the mass distribution and merger rate of CBCs. On one hand, features in the mass distribution are a highly informative component of current constraints, especially when the galaxy catalog used has low completeness over the typical range of the GW events in hand [54–58]. On the other hand, this dependence introduces a large number of additional parameters that must be constrained alongside the cosmology – up to 25 in [29]. Hence, Peak Sirens is a more direct probe of cosmology with less astrophysical entanglement.

In this letter we perform the first application of the Peak Sirens method to data using GW190814 and GW170817 (though the redshift of its host galaxy is not used) and the K-band galaxies of the GLADE+ catalog (see however [59]). As very few events lie within the depth of the GLADE+ catalog, GW170817 is included here to help demonstrate the viability of the method, even if tighter H_0 constraints might be obtained instead with its use as a bright siren. Since we have good galaxy coverage for only a limited number of GWs, we focus on the dominant parameter sensitivities: H_0 and b_{gw} .

Methodology

3D angular cross-correlations. A key assumption of this work is that GW sources are located inside galaxies, such that their positions are correlated. To study these correlations, we build pixelated galaxy and GW source sky maps using HEALPix [60, 61]. For galaxies, we decompose the radial direction in redshift bins z_i , which, together with the HEALPix pixels, fully defines voxels. We count the number of galaxies $N_g(z_i, \hat{\mathbf{n}})$ in each voxel denoted by the direction $\hat{\mathbf{n}}$ and redshift bin center z_i . We integrate the z -PDF assuming Gaussian uncertainties over each voxel. This map encodes the PDF of finding galaxies in each voxel. For the GW data, we decompose instead the radial direction in D_L bins indicated by their center D_{Lj} . We integrate the observed 3D location posterior, marginalized over other binary parameters like masses and spins, to count the fractional GW contribution to each voxel. This defines the GW map $N_{\text{gw}}(D_{Lj}, \hat{\mathbf{n}})$, which is proportional to the PDF of GW sources. With these two maps, one can compute their angular cross-correlation:

$$C_\ell(z_i, D_{Lj}) = \frac{1}{2\ell+1} \sum_{m=-\ell}^{\ell} a_{\ell m}^g(z_i) a_{\ell m}^{\text{gw}*}(D_{Lj}), \quad (1)$$

where $a_{\ell m}^g(z_i)$ and $a_{\ell m}^{\text{gw}}(D_{Lj})$ are the coefficients of their respective spherical harmonic decompositions:

$$N_X(r_{Xi}, \hat{\mathbf{n}}) = \sum_{\ell m} a_{\ell m}^i(r_{Xi}) Y_{\ell m}(\hat{\mathbf{n}}), \quad (2)$$

where in turn $X = \{\text{g}, \text{gw}\}$ for galaxies and GW sources, respectively, r_X is either z or D_L , and $Y_{\ell m}(\hat{\mathbf{n}})$ are the spherical harmonics. The resulting coefficients $C_\ell(z_i, D_{Lj})$ correspond to the 3D angular power spectrum after removing shot noise. We do not use auto-correlations in our data vector, since our focus is detecting the peak of the cross-spectrum and inferring the background cosmology from this new observable. The clustering of galaxies is a key cosmological probe of the linear perturbations; here we will use only its amplitude (and not the shape) to eliminate a global degeneracy in the power spectra between the GW and galaxy biases and the clustering amplitude σ_8 , since the cross-correlation amplitude depends on the product $b_g b_{\text{gw}} \sigma_8^2$. We find that

the clustering of GWs with current data is not yet informative due to its high shot noise, as expected [45]. We model our data vector, defined in Eq. (1), with a Gaussian likelihood,

$$\log(\mathcal{L}) = -\frac{1}{2} \sum_{\ell ij, \ell' i' j'} \Delta C_\ell^{ij} [\text{Cov}^{-1}]_{\ell ij, \ell' i' j'} \Delta C_{\ell'}^{i' j'}, \quad (3)$$

where $\Delta C_\ell^{ij} \equiv C_\ell^{\text{obs}}(z_i, D_{Lj}) - C_\ell^{\text{th}}(z_i, D_{Lj})$ denotes the difference between observed and theoretical cross-spectra.

Theoretical modelling. We use simulations to model both $C_\ell^{\text{th}}(z_i, D_{Lj}, \boldsymbol{\theta})$ in an arbitrary cosmology denoted by $\boldsymbol{\theta}$, and the covariance matrix in Eq. (3). Pairs of GW and galaxy catalogs are built in a single fiducial model $\boldsymbol{\theta}^{\text{fid}}$, with GW sources injected randomly into galaxies, as we describe in the appendix. Averaging the C_ℓ 's over simulations allows us to obtain an accurate value for $C_\ell^{\text{fid}}(z_i, D_{Lj})$. For a fixed redshift bin z_i , the cross-spectrum peaks at $D_L(z_i, \boldsymbol{\theta}^{\text{fid}})$ due to the rapid decline of the two-point correlation function of the matter field with comoving distance.

When changing continuously the cosmological parameters (here just H_0), we account for the change in this single feature, namely the position of the sharp peak in the (z, D_L) plane, while neglecting the cosmology dependence of the cross-spectrum shape, which is a sub-leading effect [50]. The position of the peak is adapted by rescaling the redshift axis of $C_\ell^{\text{fid}}(z_i, D_{Lj})$, which can be done because the mapping between z and D_L is one-to-one for a given cosmology. In doing so, a redshift in the fiducial cosmology, say z_i , corresponds to a z'_i in the $\boldsymbol{\theta}$ -cosmology, i.e. $z_i \xrightarrow{\boldsymbol{\theta}^{\text{fid}}} D_L \xrightarrow{\boldsymbol{\theta}} z'_i$, where the number of observed galaxies is also dissimilar [62]. We rescale the amplitude of the peak by the ratio of the average numbers of galaxies in corresponding bins, $\bar{N}_g(z_i)/\bar{N}_g(z'_i(\boldsymbol{\theta}))$. This method allows us to model the theoretical cross-spectrum for different cosmologies by doing simulations in only one fiducial cosmology, which we choose to be the CMB primary+lensing result of [63] (in particular, $H_0 = 67.36 \text{ km s}^{-1} \text{ Mpc}^{-1}$ and $\Omega_m = 0.3153$).

On the gravitational wave bias. The linear GW bias modulates the amplitude of the cross-correlations (see Eq. (2.16) of [50]), and as long as it varies slowly with redshift, it does not affect the position of the peak significantly. We parametrize it as $b_{\text{gw}}(1+z)$. The free parameter b_{gw} should be interpreted as the mean GW bias of the particular sample of GW sources, for which bias stochasticity can be significant [64, 65].

For Gaussian random fields, the covariance matrix of the angular power spectra depends negligibly on the bias of the lower-density field in the limit of low number density ($\bar{N}_{\text{gw}} \ll \bar{N}_g$). This is due to high shot noise of the auto-correlations. Taking the Gaussian case as inspiration, we will assume that b_{gw} enters in the likelihood only as a free factor multiplying C_ℓ^{th} , which is estimated from simulations with a fixed GW bias of 1.

Data

GLADE+ maps. We use K-band data of the GLADE+ catalog [39] to construct a galaxy number count map, $N_g(z, \hat{\mathbf{n}})$. This catalog has been widely used for GW cosmology with dark sirens [23, 25, 27, 29, 66] which allows for direct comparison with these results. We use $n_{\text{side}} = 32$ to split the sky into equal-area pixels. We fix the voxel depth to $\Delta z = 0.01$ in most of the redshift range; for $z < 0.02$, where we have precise galaxy redshifts, we use bins $3\times$ smaller instead, which is crucial to locate the cross-correlation peak of the nearest GW sources. After that, our largest bin size is of the order of the photometric redshift uncertainties that we assume to be Gaussian. It was shown in [67] that this assumption does not affect significantly current measurements of H_0 . While this simplistic choice matches current LVK dark sirens work [29], further refinements might be required when the precision on H_0 increases. Furthermore, we make a conservative cut removing all galaxies whose photo- z Gaussian PDF would have more than 0.15% support below $z = 0$.

The observed number count map $N_g(z, \hat{\mathbf{n}})$ relates to the a priori unknown *complete* galaxy map via the completeness $\hat{f}_S(z, \hat{\mathbf{n}}) \in [0, 1]$, which we estimate from the magnitude threshold $m_{\text{th}}(\hat{\mathbf{n}})$ of each pixel, following [68]:

$$\hat{f}_S(\hat{\mathbf{n}}, z) = \int_{L(m_{\text{th}}(\hat{\mathbf{n}}))}^{L_{\text{max}}} dL \phi(L) / \int_{L_{\text{min}}}^{L_{\text{max}}} dL \phi(L), \quad (4)$$

where the luminosity function $\phi(L)$ obeys a Schechter function [69]. For the GLADE+ K-band, we use L_* , L_{min} and L_{max} converted from the absolute magnitudes $M_* = -23.39$, $M_{\text{min}} = -27$ and $M_{\text{max}} = -19$, with $\alpha = -1.09$ [70]. We use the k -correction estimate [71] from the python package `kcorrect` and additional information from the J-, H- and B-bands [72]. The luminosity is then calculated via $L(M) = L_0 \cdot 10^{-2M/5}$ with $L_0 = 3.0128 \cdot 10^{28}$ W. We apply a galactic latitude mask $|b| > 20^\circ$ to get rid of star contamination close to the Milky Way. Finally, we use the publicly available code `Namaster` [73] to estimate the auto and cross-correlations from the masked data, which has after all cuts approximately 2.8×10^5 galaxies.

GWTC-3.0. Most GWs in GWTC-3.0 [74, 75] lie outside the GLADE+ redshift range, when computing $z(D_L)$ with some value of H_0 in the prior range of [20, 120]. This results in three candidates for our analysis: GW190425, GW190814, and GW170817. The first is likely a binary neutron star (BNS) merger, observed only by LIGO Livingston, resulting in poor localization. This event was thus excluded from our analysis. For the same reason, we do not consider events from GWTC-4.0 (detections from the O4a observing run), as these were generally poorly localised due to the lack of Virgo observations. The second event, GW190814, is the merger of a black-hole and a low mass compact object

and it is the best-localized event in the catalog, with area of $\Omega_{90} = 18.5 \text{ deg}^2$ at 90% CI. We have additionally GW170817, the single bright siren observed so far, whose host galaxy NGC 4993 is contained in GLADE+. We therefore focus the analysis on these last two events.

For GW190814, the GW map is built from the GW posterior obtained with the waveform IMRPhenomXPHM [76]. For GW170817, we use the GW result with PhenomPNRT with low spin prior, having fixed the sky location of the host galaxy [77, 78]. We do not use, however, any information about the measured redshift of the bright siren’s host galaxy. For convenience, we take D_L bins that correspond, in the fiducial cosmology, to the redshift binning used for galaxies. We also bin the multipoles, with bin size $\Delta\ell = 5$, which minimizes correlations introduced by the mask. We exclude the first two small- ℓ bins which are uninformative due to cosmic variance and the galactic plane mask. We further exclude scales smaller than the resolution of GW190814 ($\ell > 180 \text{ deg} / \sqrt{\Omega_{90}/\pi}$), such that our bin centers are $\ell \in \{14, 19, 24, \dots, 69\}$.

We show on the LHS of Fig. 1 a summary of the data as a weighted sum of C_ℓ ’s. The weights $w_\ell = (2\ell + 1)P_\ell(\cos(1.8^\circ))$, where P_ℓ are the Legendre polynomials, correspond to a beam with the pixel angular resolution. GW170817 and GW190814 are located, respectively, around the third D_L bin at $\simeq 40$ Mpc, and at 255 Mpc. We can identify the corresponding two peaks at redshifts $\simeq 0.008$ and $z \simeq 0.065$, the same structure one can observe on the RHS plot, which shows the theoretical prediction from almost 6000 simulations, that are described in the appendix.

Results

Significance of detection. To determine the significance of detection of cross-correlations, we take galaxy and GW maps from different simulations, such that they are uncorrelated, and compute their cross-spectrum C_ℓ^{null} , as well as its average and sample covariance. We build the $\Delta\chi^2$ distribution of these noise-only simulations to quantify how often a simulation under the null hypothesis (no cross-correlations) appears closer to the average of correlated maps than to the average of uncorrelated maps. We plot this $\Delta\chi^2$ distribution in Fig. 2 and compare with the $\Delta\chi^2$ of the data. We find that the data favors the presence of cross-correlations over noise. Fitting Fréchet distributions to each individual χ^2 of the simulations, we estimate the p-value to be 6.7×10^{-4} for cross-correlations with GW190814 only, equivalent to a two-sided Gaussian significance of 3.4σ . Adding GW170817 decreases the p-value to 1.9×10^{-9} , which is equivalent to a significance of 5.9σ .

Hubble constant and GW bias. We run MCMC chains to infer the Hubble constant and GW bias, as

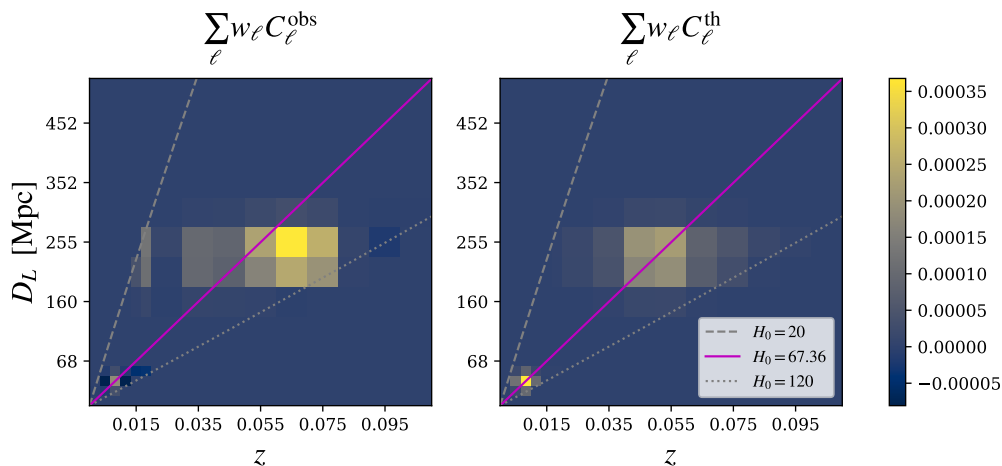


FIG. 1. Angular cross-correlations between GLADE+ and GW190814, GW170817. *Left*: Sum over multipoles $\ell \in [14, 69]$ of the C_{ℓ} s as a function of galaxy z and GW D_L . Regions corresponding to H_0 outside the prior range $[20, 120]$ $\text{km s}^{-1} \text{Mpc}^{-1}$ (grey dashed and dotted curves) are set to zero for visualization purposes. The magenta curve illustrates how the Planck cosmology compares with the data. *Right*: Same but obtained from an average over our set of simulations in the fiducial cosmology, with $b_{\text{gw}} = 2$. The bright regions correspond to the peaks in the cross-correlation signal generated by events GW170817 (bottom left corner) and GW190814 (central region) and reveal the Hubble diagram.

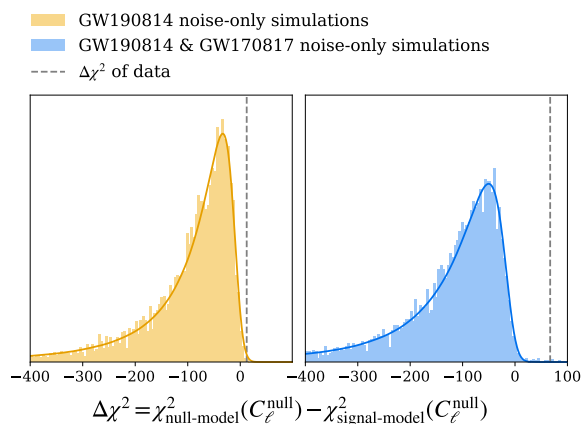


FIG. 2. $\Delta\chi^2$ between the null hypothesis (noise-only) and the model with a cross-correlation signal, for correlations with GW190814 only (left) and additionally GW170817 (right). The data (grey dashed lines) considerably prefers, with its large $\Delta\chi^2$, the signal-model against the noise-model. The solid lines are derived from the Fréchet distribution fits for the individual χ^2 histograms.

shown in Figure 3. We assume the flat priors $H_0 \in [20, 120]$ $\text{km s}^{-1} \text{Mpc}^{-1}$ and $b_{\text{gw}} \in [0, 10]$. In order to measure b_{gw} alone, we estimate b_{g} by comparing the galaxy auto-spectrum of the data with the one from the average over simulations, after removing shot noise. From the amplitude of their ratio we obtain $b_{\text{g}}(\sigma_8/\sigma_8^{\text{fid}}) = 0.85 \pm 0.13$. We then fix σ_8 to the very precise CMB measurement, $\sigma_8 = 0.8111 \pm 0.0060$ [63]. With GW190814 only, we find the following marginal-

ized constraints (highest-density intervals):

$$H_0 = 53_{-18}^{+31} \text{ km s}^{-1} \text{Mpc}^{-1} \text{ (at 68\% CI)}, \quad (5)$$

$$b_{\text{gw}} < 6.2 \text{ (at 95\% CI)}. \quad (6)$$

Adding GW170817 without its z information leads to

$$H_0 = 67_{-15}^{+18} \text{ km s}^{-1} \text{Mpc}^{-1} \text{ (at 68\% CI)}, \quad (7)$$

$$b_{\text{gw}} < 4.3 \text{ (at 95\% CI)}. \quad (8)$$

We verified from the χ^2 distribution of the simulations that our best fit in each case is a good fit to the data.

In contrast, adding GW170817 as a bright siren to the Peak Siren measurement with GW190814, one obtains $H_0 = (72 \pm 11) \text{ km s}^{-1} \text{Mpc}^{-1}$. If we instead combine the two Peak sirens with the spectral siren MLTP result from [29], which uses information from the black hole mass distribution, we obtain $H_0 = 68_{-8}^{+16} \text{ km s}^{-1} \text{Mpc}^{-1}$ as a first approximation, neglecting correlations between the two analysis. Peculiar velocity effects were not included in this work; while for galaxies they are expected to be negligible with those bin sizes, the aberration in the distances could generate a shift in H_0 which is smaller than our final uncertainties (see e.g. [79]).

We can also constrain the GW bias relative to galaxies instead of the dark matter (which is the normal implication of b_{gw}), and that does not depend on σ_8 . We find $b_{\text{gw}}/b_{\text{g}} < 8.1$ with GW190814 and $b_{\text{gw}}/b_{\text{g}} < 5.7$ with both GW190814 and GW170817. This quantity is relative to the galaxy population we are analyzing, in this case, galaxies with luminosities in the K-band, which are generally regarded as tracers of stellar mass.

Finally, we remark that the two parameters H_0 and b_{gw} have an almost transversal effect on the cross-correlations; while the first sets the peak position, the

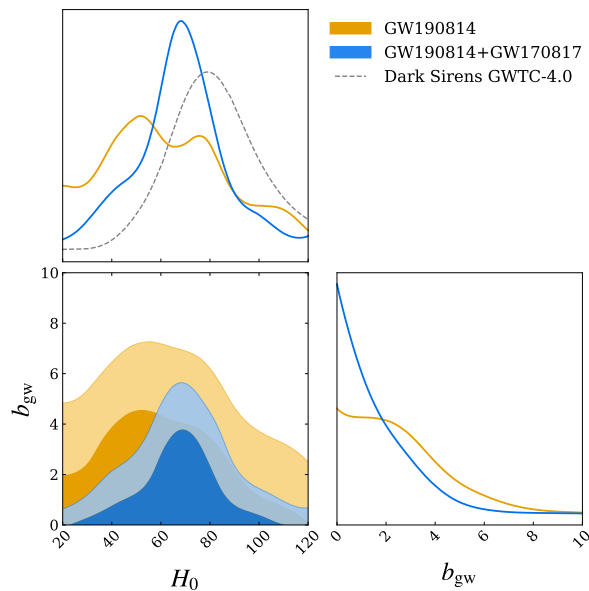


FIG. 3. 68% and 95% CI for the cross-correlations of GLADE+ with only GW190814 (orange) and with both GW190814 and the BNS GW170817 as a dark siren (blue). We also show the H_0 posterior from GWTC-4.0 dark sirens analysis (grey, dashed) for reference [29].

feature most precisely measured, the second governs its amplitude. For a fixed distance, however, the redshift of the peak also implies the number of observed galaxies at the peak, and the cross-correlation amplitude scales with $\bar{N}_g(z)$, that being the source of correlations between the two parameters. Furthermore, the triangular shape of the contours in Fig. 3 reflect the scaling of the signal-to-noise ratio with the GW bias, whose value directly impact the precision in H_0 . In addition to this degeneracy, the need to model how the covariance depends on b_{gw} as it approaches zero could be the reason why we can only place an upper bound on this parameter, despite making a significant detection of cross-correlations.

Discussion. Even with a very restricted set of only two GW events, our main result, $H_0 = 67^{+18}_{-15}$ km s $^{-1}$ Mpc $^{-1}$, is compatible and comparable with other dark siren measurements of H_0 [18, 21, 22, 25, 28, 80–82], revealing the strength of the Peak Sirens method. Assuming those events can be described by a single bias parameter at this point, we report its first observation constraint $b_{\text{gw}} < 4.3$. Although this number is subject to a high degree of stochasticity due to our small GW sample, it must be consistent with the ‘true’ GW bias, and converge to in the limit of many GW sources. GW bias will play a key role in the future as it relates to the formation mechanisms of compact objects [83], and many forecasts were made for 3G constraints [45, 47, 84–87]; our bound here marks the start of that process.

Current dark sirens results are primarily informed by

the presence of features in the mass spectrum of compact objects. In this work, when combined with GW observations, the information on H_0 comes only from the galaxy catalog. Further precision improvements can be achieved by properly combining Peak Sirens with spectral sirens. Furthermore, in the dark sirens technique, a redshift prior for GW events (constructed from a galaxy catalog) is applied along individual lines of sight within the GW sky location [88]. As such, the clustering of galaxies enters the analysis along radial lines of sight only, while the Peak Sirens approach explicitly incorporates the 3D clustering. A comprehensive study of the relation and covariance between these methods is underway.

In the simulations used in this work (see Appendix), GW host galaxies were not assumed to be necessarily in the galaxy catalog generated after applying realistic selection effects. Therefore, the modeling of the cross-correlation signal did not rely on the exact coincidence of the positions object-by-object, in line with the predictions of [50, 89]. At the same time, in those simulations we do assume that all galaxies are in principle equally likely to host a CBC. Weighting galaxies according to their chance of hosting CBCs is a component of the dark siren method that relies on modeling this probability as a function of galaxy properties such as luminosity or stellar mass [19, 90]. On one hand, this introduces more entanglement with astrophysical modeling and, on the other hand, it can enhance correlations. Here, instead, the link with galaxy properties is encoded in the GW bias [91, 92]. An alternative approach that includes galaxy weighting would require simulations where not only positions but also those properties are predicted.

In the near future, we intend to use a deeper galaxy catalog (e.g. GAIA, DESI Legacy), which has more support at the distances relevant to GWTC-4.0, since the shallowness of GLADE+ was the main limitation of the present work. Improvements are expected by including further well-localized GW events from GWTC-3.0 and eventually from the latter stages of the LVK O4 run.

As we accumulate new GW data, the precision on H_0 depends crucially on the sky position errors of GW sources. At fixed resolution, since $\bar{N}_{\text{gw}} \ll \bar{N}_g$, the signal-to-noise ratio of angular cross-spectrum in the Gaussian field approximation scales with $\sqrt{\bar{N}_{\text{gw}}}$. With 100 events with skymaps resembling GW190814, one expects a $\sim 4\%$ measurement of the H_0 using this method.

Finally, Peak Sirens is ideal for tests of gravity theories in which distances measured from GWs differ from the standard luminosity distance [9, 26, 27, 93–100]. We plan to use this method to measure the dark energy equation of state and the friction induced in tensor modes. This work represents the first stone of a castle of many opportunities, which are left for future work.

Acknowledgments. We would like to thank Fabien Lacasa, Louis Legrand, Konstantin Leyde, Kr-

ishna Naidoo, Riccardo Sturani, Nicolas Tessore and Michael Williams for useful discussions and insights. We also thank Nicola Borghi, David Alonso and Maciej Bilicki for comments on the draft. I.S.M., C.D. and T.B. are supported by ERC Starting Grant SHADE (grant no. StG 949572). I.S.M. also acknowledges funding from FAPESP. T.B. is further supported by a Royal Society University Research Fellowship (grant no. URF\R\231006). R.A. is supported by FAPESP and CNPq. J. F. would like to thank CNPq for financial support. M.Q. is supported by the Brazilian research agencies FAPERJ project E-26/201.237/2022, CNPq and CAPES. This material is based upon work supported by NSF’s LIGO Laboratory which is a major facility fully funded by the National Science Foundation.

Supporting research data are available on reasonable request from the corresponding authors. For the purpose of open access, the author(s) have applied a Creative Commons Attribution (CC-BY) license to any Author Accepted Manuscript version arising.

Appendix: Simulations

Galaxy simulations. We use the code GLASS [101] to perform galaxy simulations. We give as an inputs: the 3D matter power spectrum obtained from CAMB [102] in the fiducial cosmology, the galaxy bias $b_g = 1 + z$ and the total number of galaxies in each redshift bin. The code builds a lognormal field on the light-cone that has these properties. Hence, we simulate a complete version of the GLADE+ catalogs, meaning that we generate $N_c(z)$ galaxies. This profile is slightly deformed with respect to the estimate from the completeness fraction, due to photo- z smearing, such that the final redshift distribution recovers the observed one. We use this completed galaxy map to draw the GW host galaxies. The final map, which will mimic only the observed galaxies will therefore not necessarily contain the GW host galaxies.

We then build an observed version $N_g(z, \hat{n})$ of this catalog, which is masked around the Milky Way, like the data. Since no luminosity function is assigned to galaxies in our simulations, to model a magnitude-limited survey, we exclude galaxies proportionally to the completeness map in each pixel and redshift bin. We then draw a number count from a Poisson distribution centered around the number of remaining galaxies in each voxel. Finally, based on the observed fraction of galaxies with photometric redshifts, we sample an updated redshift from a Gaussian and integrate the PDF of these galaxies over each voxel to match what is done with the data, while keeping the fraction of spectroscopic galaxies point-like.

Gravitational wave simulations. We perform constrained simulations which enforce the statistical properties of the true data sets, that is, we always simulate

the “same” GW events, but as if they were happening in different galaxies. Due to the small number of GW events, we fix the angular and radial resolutions of the simulated GW events to be the same as those, but sample the radial and sky positions randomly as follows. First, for each GW in each simulation, we draw from the real data marginalized D_L posterior the true value of D_L for that simulation. We then convert the latter to a redshift using the fiducial cosmology. The sky position is found by randomly picking a host galaxy from the corresponding redshift bin z_i . Given this “true” position of the GW event, its 3D posterior is placed such that the peak of the distribution coincides with the sky position of the host galaxy. Finally, we draw from this distribution to obtain the “measured” position of the GW event, and re-center the distribution around that. We assume a simple scenario where all galaxies are equally likely to host a GW, and therefore, $b_{gw}/b_g = 1$ is the fiducial value in the simulations; folding in correlations between galaxy properties and the probability of hosting is left for future work.

Since the two events considered were observed well outside the masked region, we exclude simulations where they fall more than 5% volume-wise in the mask, in order to avoid an over-estimation of the covariance matrix. The anisotropic antenna patterns of the detectors are not being reproduced in our simulations, for simplicity, as with only a small number of events, anisotropies in the GW distribution are dominated by shot noise. We generated almost 6000 simulations, from which the covariance in Eq. (3) could be accurately estimated.

* isabela.matos@port.ac.uk

† charles.dalang@ens.fr

‡ tessa.baker@port.ac.uk

§ raulabramo@usp.br

¶ joao.vitor.ferri@usp.br

** mqmartin@cbpf.br

- [1] S. Mastrogiovanni, C. Karathanasis, J. Gair, G. Ashton, S. Rinaldi, H.-Y. Huang, and G. Dálya, *Annalen Phys.* **536**, 2200180 (2024).
- [2] T. A. Callister, Observed Gravitational-Wave Populations (2024), [arXiv:2410.19145](https://arxiv.org/abs/2410.19145) [astro-ph.HE].
- [3] B. F. Schutz, *Nature* **323**, 310 (1986).
- [4] D. E. Holz and S. A. Hughes, *Astrophys. J.* **629**, 15 (2005), [arXiv:astro-ph/0504616](https://arxiv.org/abs/astro-ph/0504616).
- [5] N. Dalal, D. E. Holz, S. A. Hughes, and B. Jain, *Phys. Rev. D* **74**, 063006 (2006), [arXiv:astro-ph/0601275](https://arxiv.org/abs/astro-ph/0601275).
- [6] S. Nissanke, D. E. Holz, S. A. Hughes, N. Dalal, and J. L. Sievers, *Astrophys. J.* **725**, 496 (2010), [arXiv:0904.1017](https://arxiv.org/abs/0904.1017) [astro-ph.CO].
- [7] S. Nissanke, D. E. Holz, N. Dalal, S. A. Hughes, J. L. Sievers, and C. M. Hirata, Determining the Hubble constant from gravitational wave observations of merging compact binaries (2013), [arXiv:1307.2638](https://arxiv.org/abs/1307.2638) [astro-ph.CO].

- [8] V. Alfradique, M. Quartin, L. Amendola, T. Castro, and A. Toubiana, *Mon. Not. Roy. Astron. Soc.* **517**, 5449 (2022), arXiv:2205.14034 [astro-ph.CO].
- [9] I. Matos, M. Quartin, L. Amendola, M. Kunz, and R. Sturani, *JCAP* **08**, 007, arXiv:2311.17176 [astro-ph.CO].
- [10] C. L. MacLeod and C. J. Hogan, *Phys. Rev. D* **77**, 043512 (2008), arXiv:0712.0618 [astro-ph].
- [11] W. Del Pozzo, *Phys. Rev. D* **86**, 043011 (2012), arXiv:1108.1317 [astro-ph.CO].
- [12] I. Mandel, W. M. Farr, and J. R. Gair, *Mon. Not. Roy. Astron. Soc.* **486**, 1086 (2019), arXiv:1809.02063 [physics.data-an].
- [13] S. Borhanian, A. Dhani, A. Gupta, K. G. Arun, and B. S. Sathyaprakash, *Astrophys. J. Lett.* **905**, L28 (2020), arXiv:2007.02883 [astro-ph.CO].
- [14] B. P. Abbott *et al.* (LIGO Scientific, Virgo, Fermi-GBM, INTEGRAL), *Astrophys. J. Lett.* **848**, L13 (2017), arXiv:1710.05834 [astro-ph.HE].
- [15] B. P. Abbott *et al.* (LIGO Scientific, Virgo, 1M2H, Dark Energy Camera GW-E, DES, DLT40, Las Cumbres Observatory, VINROUGE, MASTER), *Nature* **551**, 85 (2017), arXiv:1710.05835 [astro-ph.CO].
- [16] M. Fishbach *et al.* (LIGO Scientific, Virgo), *Astrophys. J. Lett.* **871**, L13 (2019), arXiv:1807.05667 [astro-ph.CO].
- [17] M. Soares-Santos *et al.* (DES, LIGO Scientific, Virgo), *Astrophys. J. Lett.* **876**, L7 (2019), arXiv:1901.01540 [astro-ph.CO].
- [18] A. Palmese *et al.* (DES), *Astrophys. J. Lett.* **900**, L33 (2020), arXiv:2006.14961 [astro-ph.CO].
- [19] R. Gray, I. M. n. Hernandez, H. Qi, A. Sur, P. R. Brady, H.-Y. Chen, W. M. Farr, M. Fishbach, J. R. Gair, A. Ghosh, D. E. Holz, S. Mastrogiovanni, C. Messenger, D. A. Steer, and J. Veitch, *Phys. Rev. D* **101**, 122001 (2020).
- [20] M. Quartin, L. Amendola, and B. Moraes, *Mon. Not. Roy. Astron. Soc.* **512**, 2841 (2022), arXiv:2111.05185 [astro-ph.CO].
- [21] A. Finke, S. Foffa, F. Iacovelli, M. Maggiore, and M. Mancarella, *JCAP* **08**, 026, arXiv:2101.12660 [astro-ph.CO].
- [22] A. Palmese, C. R. Bom, S. Mucesh, and W. G. Hartley, *Astrophys. J.* **943**, 56 (2023), arXiv:2111.06445 [astro-ph.CO].
- [23] R. Gray *et al.*, *JCAP* **12**, 023, arXiv:2308.02281 [astro-ph.CO].
- [24] B. P. Abbott *et al.* (LIGO Scientific, Virgo, VIRGO), *Astrophys. J.* **909**, 218 (2021), arXiv:1908.06060 [astro-ph.CO].
- [25] R. Abbott *et al.* (LIGO Scientific, Virgo, KAGRA), *Astrophys. J.* **949**, 76 (2023), arXiv:2111.03604 [astro-ph.CO].
- [26] K. Leyde, S. Mastrogiovanni, D. A. Steer, E. Chassande-Mottin, and C. Karathanasis, *JCAP* **09**, 012, arXiv:2202.00025 [gr-qc].
- [27] A. Chen, R. Gray, and T. Baker, *JCAP* **02**, 035, arXiv:2309.03833 [gr-qc].
- [28] C. R. Bom, V. Alfradique, A. Palmese, G. Teixeira, L. Santana-Silva, A. Santos, and P. Darc, *Mon. Not. Roy. Astron. Soc.* **535**, 961 (2024), arXiv:2404.16092 [astro-ph.CO].
- [29] A. G. Abac *et al.* (LIGO Scientific, VIRGO, KAGRA), GWTC-4.0: Constraints on the Cosmic Expansion Rate and Modified Gravitational-wave Propagation (2025), arXiv:2509.04348 [astro-ph.CO].
- [30] B. P. Abbott *et al.* (KAGRA, LIGO Scientific, Virgo), *Living Rev. Rel.* **19**, 1 (2016), arXiv:1304.0670 [gr-qc].
- [31] J. Aasi *et al.* (LIGO Scientific), *Class. Quant. Grav.* **32**, 074001 (2015), arXiv:1411.4547 [gr-qc].
- [32] F. Acernese *et al.* (VIRGO), *Class. Quant. Grav.* **32**, 024001 (2015), arXiv:1408.3978 [gr-qc].
- [33] T. Akutsu *et al.* (KAGRA), *PTEP* **2021**, 05A101 (2021), arXiv:2005.05574 [physics.ins-det].
- [34] Y. Aso, Y. Michimura, K. Somiya, M. Ando, O. Miyakawa, T. Sekiguchi, D. Tatsumi, and H. Yamamoto (KAGRA), *Phys. Rev. D* **88**, 043007 (2013), arXiv:1306.6747 [gr-qc].
- [35] K. Somiya (KAGRA), *Class. Quant. Grav.* **29**, 124007 (2012), arXiv:1111.7185 [gr-qc].
- [36] A. G. Abac *et al.* (LIGO Scientific, VIRGO, KAGRA), GWTC-4.0: Updating the Gravitational-Wave Transient Catalog with Observations from the First Part of the Fourth LIGO-Virgo-KAGRA Observing Run (2025), arXiv:2508.18082 [gr-qc].
- [37] E. Capote *et al.*, *Phys. Rev. D* **111**, 062002 (2025), arXiv:2411.14607 [gr-qc].
- [38] S. Soni *et al.* (LIGO), *Class. Quant. Grav.* **42**, 085016 (2025), arXiv:2409.02831 [astro-ph.IM].
- [39] G. Dálya *et al.*, *Mon. Not. Roy. Astron. Soc.* **514**, 1403 (2022), arXiv:2110.06184 [astro-ph.CO].
- [40] S. Mukherjee and B. D. Wandelt, Beyond the classical distance-redshift test: cross-correlating redshift-free standard candles and sirens with redshift surveys (2018), arXiv:1808.06615 [astro-ph.CO].
- [41] S. Mukherjee, B. D. Wandelt, S. M. Nissanke, and A. Silvestri, *Phys. Rev. D* **103**, 043520 (2021), arXiv:2007.02943 [astro-ph.CO].
- [42] C. C. Diaz and S. Mukherjee, *Mon. Not. Roy. Astron. Soc.* **511**, 2782 (2022), arXiv:2107.12787 [astro-ph.CO].
- [43] J. Fonseca, S. Zazzera, T. Baker, and C. Clarkson, *JCAP* **08**, 050, [Erratum: *JCAP* **06**, E02 (2024)], arXiv:2304.14253 [astro-ph.CO].
- [44] A. Balaudo, M. Pantiri, and A. Silvestri, *JCAP* **02**, 023, arXiv:2311.17904 [astro-ph.CO].
- [45] S. Zazzera, J. Fonseca, T. Baker, and C. Clarkson, *Mon. Not. Roy. Astron. Soc.* **537**, 1912 (2025), arXiv:2412.01678 [astro-ph.CO].
- [46] S. Afroz and S. Mukherjee, *Mon. Not. Roy. Astron. Soc.* **534**, 1283 (2024), arXiv:2407.09262 [astro-ph.CO].
- [47] A. Pedrotti, M. Mancarella, J. Bel, and D. Gerosa, Cosmology with the angular cross-correlation of gravitational-wave and galaxy catalogs: forecasts for next-generation interferometers and the Euclid survey (2025), arXiv:2504.10482 [astro-ph.CO].
- [48] G. Sala, A. Cuoco, J. Lesgourgues, K.-R. Revis, L. Valbusa Dall'Armi, and S. Casas, Inferring cosmological parameters from galaxy and dark sirens cross-correlation (2025), arXiv:2510.08699 [astro-ph.CO].
- [49] J. Pan, D. Huterer, C. Avestruz, D. H. T. Cheung, E. Trott, N. Dalal, and D. Jeong, Determining the Hubble Constant through Cross-Correlation of Galaxies and Gravitational Waves (2025), arXiv:2510.19931 [astro-ph.CO].
- [50] J. Ferri, I. L. Tashiro, L. R. Abramo, I. Matos, M. Quartin, and R. Sturani, *JCAP* **04**, 008, arXiv:2412.00202 [astro-ph.CO].
- [51] M. Oguri, *Monthly Notices of the Royal Astronomical*

- Society **480**, 3842–3855 (2018).
- [52] J. A. Newman, *Astrophys. J.* **684**, 88 (2008), [arXiv:0805.1409 \[astro-ph\]](#).
- [53] E. Di Valentino, O. Mena, S. Pan, L. Visinelli, W. Yang, A. Melchiorri, D. F. Mota, A. G. Riess, and J. Silk, *Class. Quant. Grav.* **38**, 153001 (2021), [arXiv:2103.01183 \[astro-ph.CO\]](#).
- [54] J. M. Ezquiaga and D. E. Holz, *Phys. Rev. Lett.* **129**, 061102 (2022), [arXiv:2202.08240 \[astro-ph.CO\]](#).
- [55] G. Pierra, S. Mastrogiovanni, S. Perriès, and M. Mapelli, *Phys. Rev. D* **109**, 083504 (2024), [arXiv:2312.11627 \[astro-ph.CO\]](#).
- [56] Y.-J. Li, S.-P. Tang, Y.-Z. Wang, and Y.-Z. Fan, *Astrophys. J.* **976**, 153 (2024), [arXiv:2406.11607 \[astro-ph.CO\]](#).
- [57] A. M. Farah, T. A. Callister, J. M. Ezquiaga, M. Zevin, and D. E. Holz, *Astrophys. J.* **978**, 153 (2025), [arXiv:2404.02210 \[astro-ph.CO\]](#).
- [58] I. Magaña Hernandez and A. Palmese, Spectral siren cosmology from gravitational-wave observations in GWTC-4.0 (2025), [arXiv:2509.03607 \[astro-ph.CO\]](#).
- [59] We note that an attempt to detect the GW-galaxy cross-correlation signal using similar data sets was presented in [103], but returning a null result. This work has various differences in methodology compared to ours, which do not allow it to precisely locate the peak of GW-galaxy correlations computed in pairs of thin and widely separated radial shells.
- [60] A. Zonca, L. Singer, D. Lenz, M. Reinecke, C. Rosset, E. Hivon, and K. Gorski, *Journal of Open Source Software* **4**, 1298 (2019).
- [61] K. M. Górski, E. Hivon, A. J. Banday, B. D. Wandelt, F. K. Hansen, M. Reinecke, and M. Bartelmann, *ApJ* **622**, 759 (2005), [arXiv:astro-ph/0409513](#).
- [62] That differs slightly from [50], where instead distance bins are rescaled, i.e. $C_\ell^{\text{th}}(z_i, D_{Lj}, \theta) = C_\ell^{\text{fid}}(z_i, z(D_{Lj}, \theta))$. In this work, we rescale the galaxy redshift bins according to the new cosmology. This is more robust against the density profiles of each GW event since there are very few GW events versus an abundant numbers of galaxies.
- [63] N. Aghanim *et al.* (Planck), *Astron. Astrophys.* **641**, A6 (2020), [Erratum: *Astron. Astrophys.* 652, C4 (2021)], [arXiv:1807.06209 \[astro-ph.CO\]](#).
- [64] A. Dekel and O. Lahav, *Astrophys. J.* **520**, 24 (1999), [arXiv:astro-ph/9806193 \[astro-ph\]](#).
- [65] A. Paranjape, O. Hahn, and R. K. Sheth, *Mon. Not. Roy. Astron. Soc.* **476**, 3631 (2018), [arXiv:1706.09906 \[astro-ph.CO\]](#).
- [66] S. Mastrogiovanni, D. Laghi, R. Gray, G. C. Santoro, A. Ghosh, C. Karathanasis, K. Leyde, D. A. Steer, S. Perriès, and G. Pierra, *Phys. Rev. D* **108**, 042002 (2023), [arXiv:2305.10488 \[astro-ph.CO\]](#).
- [67] C. Turcki, M. Bilicki, G. Dálya, R. Gray, and A. Ghosh, *Mon. Not. Roy. Astron. Soc.* **526**, 6224 (2023), [arXiv:2302.12037 \[gr-qc\]](#).
- [68] R. Gray, C. Messenger, and J. Veitch, *Mon. Not. Roy. Astron. Soc.* **512**, 1127 (2022), [arXiv:2111.04629 \[astro-ph.CO\]](#).
- [69] P. Schechter, *Astrophys. J.* **203**, 297 (1976).
- [70] C. S. Kochanek, M. A. Pahre, E. E. Falco, J. P. Huchra, J. Mader, T. H. Jarrett, T. Chester, R. Cutri, and S. E. Schneider, *Astrophys. J.* **560**, 566 (2001), [arXiv:astro-ph/0011456](#).
- [71] D. W. Hogg, I. K. Baldry, M. R. Blanton, and D. J. Eisenstein, The K correction (2002), [arXiv:astro-ph/0210394](#).
- [72] M. R. Blanton and S. Roweis, *Astron. J.* **133**, 734 (2007), [arXiv:astro-ph/0606170](#).
- [73] D. Alonso, J. Sanchez, and A. Slosar (LSST Dark Energy Science), *Mon. Not. Roy. Astron. Soc.* **484**, 4127 (2019), [arXiv:1809.09603 \[astro-ph.CO\]](#).
- [74] R. Abbott *et al.* (KAGRA, VIRGO, LIGO Scientific), *Phys. Rev. X* **13**, 041039 (2023), [arXiv:2111.03606 \[gr-qc\]](#).
- [75] A. Buikema *et al.*, *Phys. Rev. D* **102**, 062003 (2020).
- [76] LIGO Scientific Collaboration, GWTC-2.1: Deep extended catalog of compact binary coalescences observed by LIGO and Virgo during the first half of the third observing run, <https://dcc.ligo.org/LIGO-P2100063/public> ().
- [77] LIGO Scientific Collaboration, Properties of the binary neutron star merger GW170817, <https://dcc.ligo.org/LIGO-P1800061/public> ().
- [78] B. P. Abbott *et al.* (LIGO Scientific, Virgo), *Phys. Rev. X* **9**, 011001 (2019), [arXiv:1805.11579 \[gr-qc\]](#).
- [79] C. Nicolaou, O. Lahav, P. Lemos, W. Hartley, and J. Braden, *Mon. Not. Roy. Astron. Soc.* **495**, 90 (2020), [arXiv:1909.09609 \[astro-ph.CO\]](#).
- [80] W. Ballard *et al.* (DESI), *Res. Notes AAS* **7**, 250 (2023), [arXiv:2311.13062 \[astro-ph.CO\]](#).
- [81] S. Vasylyev and A. Filippenko, *Astrophys. J.* **902**, 149 (2020), [arXiv:2007.11148 \[astro-ph.CO\]](#).
- [82] V. Alfradique *et al.*, *Mon. Not. Roy. Astron. Soc.* **528**, 3249 (2024), [arXiv:2310.13695 \[astro-ph.CO\]](#).
- [83] G. Scelfo, N. Bellomo, A. Raccanelli, S. Matarrese, and L. Verde, *JCAP* **09**, 039, [arXiv:1809.03528 \[astro-ph.CO\]](#).
- [84] S. Libanore, M. C. Artale, D. Karagiannis, M. Liguori, N. Bartolo, Y. Bouffanais, N. Giacobbo, M. Mapelli, and S. Matarrese, *JCAP* **02**, 035, [arXiv:2007.06905 \[astro-ph.CO\]](#).
- [85] S. Libanore, M. C. Artale, D. Karagiannis, M. Liguori, N. Bartolo, Y. Bouffanais, M. Mapelli, and S. Matarrese, *JCAP* **02** (02), 003, [arXiv:2109.10857 \[astro-ph.CO\]](#).
- [86] S. Zazzera, J. Fonseca, T. Baker, and C. Clarkson, Exploring future synergies for large-scale structure between gravitational waves and radio sources (2025), [arXiv:2505.15645 \[astro-ph.CO\]](#).
- [87] A. Abac *et al.* (ET), The Science of the Einstein Telescope (2025), [arXiv:2503.12263 \[gr-qc\]](#).
- [88] R. Gray, C. Messenger, and J. Veitch, *Monthly Notices of the Royal Astronomical Society* **512**, 1127 (2022), <https://academic.oup.com/mnras/article-pdf/512/1/1127/45303118/stac366.pdf>.
- [89] S. Bera, D. Rana, S. More, and S. Bose, *Astrophys. J.* **902**, 79 (2020), [arXiv:2007.04271 \[astro-ph.CO\]](#).
- [90] M. Pálfi, G. Dálya, and P. Raffai, *Mon. Not. Roy. Astron. Soc.* **539**, 1879 (2025), [arXiv:2503.20777 \[astro-ph.GA\]](#).
- [91] A. Dehghani, J. L. Kim, D. S. Hosseini, A. Krolewski, S. Mukherjee, and G. Geshnizjani, *JCAP* **04**, 056, [arXiv:2411.11965 \[astro-ph.GA\]](#).
- [92] D. S. Hosseini, A. Dehghani, J. L. Kim, A. Krolewski, S. Mukherjee, and G. Geshnizjani, Modeling Gravitational Wave Bias from 3D Power Spectra of Spectroscopic Surveys (2025), [arXiv:2506.11201 \[astro-ph.GA\]](#).

- [93] L. Lombriser and A. Taylor, *JCAP* **03**, 031, [arXiv:1509.08458 \[astro-ph.CO\]](#).
- [94] I. D. Saltas, I. Sawicki, L. Amendola, and M. Kunz, *Phys. Rev. Lett.* **113**, 191101 (2014), [arXiv:1406.7139 \[astro-ph.CO\]](#).
- [95] L. Amendola, I. Sawicki, M. Kunz, and I. D. Saltas, *JCAP* **08**, 030, [arXiv:1712.08623 \[astro-ph.CO\]](#).
- [96] E. Belgacem, Y. Dirian, S. Foffa, and M. Maggiore, *Phys. Rev. D* **98**, 023510 (2018), [arXiv:1805.08731 \[gr-qc\]](#).
- [97] A. Nishizawa, *Phys. Rev. D* **97**, 104037 (2018), [arXiv:1710.04825 \[gr-qc\]](#).
- [98] T. Baker and I. Harrison, *JCAP* **01**, 068, [arXiv:2007.13791 \[astro-ph.CO\]](#).
- [99] E. Colangeli, K. Leyde, and T. Baker, *JCAP* **05**, 078, [arXiv:2501.05560 \[gr-qc\]](#).
- [100] S. Mukherjee, B. D. Wandelt, and J. Silk, *Mon. Not. Roy. Astron. Soc.* **502**, 1136 (2021), [arXiv:2012.15316 \[astro-ph.CO\]](#).
- [101] N. Tessore, A. Loureiro, B. Joachimi, M. von Wietersheim-Kramsta, and N. Jeffrey, *The Open Journal of Astrophysics* **6**, 11 (2023), [arXiv:2302.01942 \[astro-ph.CO\]](#).
- [102] A. Lewis and A. Challinor, CAMB: Code for Anisotropies in the Microwave Background, Astrophysics Source Code Library, record ascl:1102.026 (2011).
- [103] S. Mukherjee, A. Krolewski, B. D. Wandelt, and J. Silk, *Astrophys. J.* **975**, 189 (2024), [arXiv:2203.03643 \[astro-ph.CO\]](#).